



Published in final edited form as:

*Magn Reson Imaging*. 2009 December ; 27(10): 1370–1381. doi:10.1016/j.mri.2009.05.048.

## Functional MRI brain activation directly from $k$ -space

Daniel B. Rowe<sup>a,b,\*</sup>, Andrew D. Hahn<sup>a</sup>, and Andrew S. Nencka<sup>a</sup>

<sup>a</sup>Department of Biophysics, Medical College of Wisconsin, Milwaukee, WI 53226, USA

<sup>b</sup>Division of Biostatistics, Medical College of Wisconsin, Milwaukee, WI 53226, USA

### Abstract

In functional magnetic resonance imaging (fMRI), the process of determining statistically significant brain activation is commonly performed in terms of voxel time series measurements after image reconstruction and magnitude-only time series formation. The image reconstruction and statistical activation processes are treated separately. In this manuscript, a framework is developed so that statistical analysis is performed in terms of the original, pre-reconstruction, complex-valued  $k$ -space measurements. First, the relationship between complex-valued (Fourier) encoded  $k$ -space measurements and complex-valued image measurements from (Fourier) reconstructed images is reviewed. Second, the voxel time-series measurements are written in terms of the original spatio-temporal  $k$ -space measurements utilizing this  $k$ -space and image relationship. Finally, voxel-wise fMRI activation can be determined in image space in terms of the original  $k$ -space measurements. Additionally, the spatio-temporal covariance between reconstructed complex-valued voxel time series can be written in terms of the spatio-temporal covariance between complex-valued  $k$ -space measurements. This allows one to utilize the originally measured data in its more natural, acquired state rather than in a transformed state. The effects of modeling preprocessing in  $k$ -space on voxel activation and correlation can then be examined.

### Keywords

image reconstruction;  $k$ -space; fMRI; complex data; Rowe-Logan

## 1. Introduction

In functional magnetic resonance imaging (fMRI), an array of data for an individual image is observed in an encoded form. The sampled data are generally Fourier encoded [2,4] and thus are measured spatial frequencies. These spatial frequency ( $k$ -space) observations are then reconstructed into an individual image array by the process of an inverse Fourier transformation. A series of these arrays of encoded images are acquired and the reconstruction process is applied to each array. For each voxel, temporally sequential voxel measurements are collected into a time series for determination of statistically significant activation. The originally sampled spatial frequencies are complex-valued and the inverse Fourier transformation image reconstruction process may yield complex-valued data. Due to

---

\*Corresponding author. Daniel B. Rowe, Department of Biophysics, Medical College of Wisconsin, 8701 Watertown Plank Road, Milwaukee, WI 53226, Tel: +1 414 456 4027, fax: +1 414 456 6512, *Email address*: dbrowe@mcw.edu (D.B. Rowe).

**Publisher's Disclaimer:** This is a PDF file of an unedited manuscript that has been accepted for publication. As a service to our customers we are providing this early version of the manuscript. The manuscript will undergo copyediting, typesetting, and review of the resulting proof before it is published in its final citable form. Please note that during the production process errors may be discovered which could affect the content, and all legal disclaimers that apply to the journal pertain.

measurement error and imperfections in the Fourier encoding, voxel time series are generally complex-valued.

The process of determining statistical activation in each voxel has, for the most part, been from magnitude-only time series [1,12]. The process of converting a complex-valued time series into a magnitude-only time series is to take the square root of the sum of the squares of the real and imaginary parts of the complex-valued time series at each time point [11]. An activation statistic from the magnitude-only time series for each voxel is determined by computing a measure of association between the observed voxel time series and a preassigned ideal time series based on the timing of the experiment and physiological considerations. This association measure for each voxel is statistically compared to the association measure that would result from a time series of random noise. A statistical threshold is chosen, a scale of color values for the activation statistic is assigned, and each voxel above threshold is given the color corresponding to its activation statistic.

The idea of computing an activation statistic from the complex-valued time series has been previously discussed [5,8]. This idea of computing fMRI activation from complex-valued data has recently been expanded upon [9-12]. Work has also been performed on computing fMRI activation from phase-only time series [13]. However, the processes of image reconstruction and statistical activation have been treated separately. Thus, activation is determined in terms of complex-valued voxel measurements after reconstruction and not the original encoded measurements.

In the current study, the relationship between the original encoded  $k$ -space measurements and reconstructed voxel measurements for each image is summarized. For each image, a vector of real-imaginary reconstructed voxel measurements is formed and written as a linear combination of real-imaginary  $k$ -space measurements. A larger vector of reconstructed real-imaginary voxel time series measurements is formed by stacking the individual vectors of real-imaginary voxel measurements for each image in temporal order. This large vector is written as a linear combination of a large vector of real-imaginary  $k$ -space time series measurements that is ordered in a similar manner. A permutation matrix is utilized to reorder the voxel measurements that are real then imaginary per image to be of real then imaginary per voxel. Statistical functional brain activation can then be determined with the aforementioned recent complex-valued activation models. A map of these activation statistics can then be thresholded to determine statistically significant activation while adjusting for multiple comparisons [6, 7].

Statistically significant voxel activation and correlation between voxels can thus be determined in image space in terms of the originally acquired  $k$ -space measurements. This will allow the modeling of the originally acquired measurements in their original state, as they are acquired, and not in a transformed state. Implications of  $k$ -space preprocessing on voxel activation and correlation can then be evaluated.

## 2. Background

Previous work has included the development of a real-valued representation of the standard complex-valued Fourier transform [14]. In this section we review the representation and offer a graphical example to illustrate the method. Magnetic resonance images are almost exclusively Fourier encoded. That is, one ideally measures the Fourier transform of an image and reconstruct the image via an inverse Fourier transform. The Fourier transform and inverse Fourier transforms are complex-valued procedures that results in complex-valued arrays.

Standard, complex-valued Fourier matrices are defined as follows. If  $\Omega_C$  is a  $p \times p$  Fourier matrix, it is a matrix with  $(j,k)^{\text{th}}$  element  $[\Omega_C]_{jk} = \kappa (\omega^{jk})$  where  $\kappa=1$  and  $\omega = \exp[-i 2 \pi (j-1)$

$(k-1)/p]$  for the forward transformation while  $\kappa=1/p$  and  $\omega = \exp[+i 2\pi (j-1)(k-1)/p]$  for the inverse transformation, where  $j,k=1,\dots,p$ .

Consider the Fourier transform of an image that has dimensions  $p_y \times p_x$  ( $p_y$  rows and  $p_x$  columns). Often the image is square, although this is not necessary. More specifically, consider an  $8 \times 8$ , ideal, noiseless, gray scale image as presented in Fig. 1. Since the Fourier transform and inverse Fourier transform procedures operate on, and produce complex-valued arrays, the real-valued image in Fig. 1 can be represented as a complex-valued image  $R_C$  that has a real part  $R_R$  as in Fig. 1 an imaginary part  $R_I$  that is the zero matrix so that  $R_C = R_R + iR_I$ . The encoded data, or Fourier transform of this image, can be found as in Eq. (1) by pre-multiplying the  $p_y \times p_x$  dimensional complex-valued matrix  $R_C$  by a standard complex-valued forward Fourier matrix  $\Omega_{yC} = \Omega_{yR} + i\Omega_{yI}$ , that is of dimensions  $p_y \times p_y$ , and post-multiplying  $R_C$  by the transpose of another standard forward Fourier matrix  $\bar{\Omega}_{xT} = (\bar{\Omega}_{xR} + i\bar{\Omega}_{xI})^T$ , where T denotes matrix transposition, that is of dimensions  $p_x \times p_x$ . The result of the pre- and post-multiplications is a complex-valued array of spatial frequency ( $k$ -space) measurements,  $S_C$ , with real part  $S_R$  and imaginary part  $S_I$  as also shown in Eq. (1).

$$(\bar{\Omega}_{yR} + i\bar{\Omega}_{yI})(R_R + iR_I)(\bar{\Omega}_{xR} + i\bar{\Omega}_{xI})^T = (S_R + iS_I) \quad (1)$$

This mathematical procedure is graphically illustrated in Fig. 2 using the aforementioned  $8 \times 8$  image. In Fig. 2 the  $8 \times 8$  image,  $R_C$ , is utilized to mimic an image from a magnetic resonance echo planar imaging experiment.  $R_C$  is displayed with real part,  $R_R$ , in Fig. 2c and imaginary part,  $R_I$ , in Fig. 2d. The spatial frequency ( $k$ -space) values,  $S_C = (S_R + iS_I)$ , associated with this complex-valued image, are found by pre-multiplying the complex-valued image by the complex-valued forward Fourier matrix  $\Omega_{yC}$  (Fig. 2a and Fig 2b) and then post-multiplying the result by the transpose of the symmetric forward Fourier matrix (Fig. 2e and Fig. 2f). The spatial frequency ( $k$ -space) values,  $S_C$ , for the complex-valued image  $R_C$  are presented as an image with real part,  $S_R$ , in Fig. 2g and imaginary part,  $S_I$ , in Fig. 2h. Note that, as mentioned earlier, the image does not have to be square.

However, as previously described, in MRI encoded ( $k$ -space) measurements,  $S_C$ , are made and reconstructed (transformed) into an image. The inverse Fourier procedure is performed. This reconstruction procedure, or inverse Fourier transform, of the spatial frequency ( $k$ -space) measurements can be found as

$$(\Omega_{yR} + i\Omega_{yI})(S_R + iS_I)(\Omega_{xR} + i\Omega_{xI})^T = (R_R + iR_I) \quad (2)$$

by pre-multiplying the  $p_y \times p_x$  dimensional complex-valued spatial frequency matrix,  $S_C$ , by a complex-valued inverse Fourier matrix,  $\Omega_y$ , that is of dimensions  $p_y \times p_y$ , and post-multiplying  $S_C$  by the transpose of another Fourier matrix,  $\bar{\Omega}_x^T$ , that is of dimensions  $p_x \times p_x$ , where T denotes matrix transposition. The result of the pre- and post-multiplications is a complex-valued array of image measurements  $R_C$ , with real part  $R_R$  and imaginary part  $R_I$  as also shown in Eq. (2).

The complex-valued image  $R_C$  can be recovered as seen in Fig. 3. The process of recovering the original complex-valued image  $R_C$  is to pre-multiply the complex-valued spatial frequency ( $k$ -space) values  $S_C$  by the complex-valued inverse Fourier matrix  $\Omega_{yC}$ , (Fig. 3a and Fig. 3b) then post-multiply the result by the transpose of the symmetric inverse Fourier matrix  $\Omega_{xT}$ ,

(Fig. 3e and Fig. 3f). The recovered complex-valued image,  $R_C$ , is presented with real part,  $R_R$ , in Fig. 3g and imaginary part,  $R_I$ , in Fig. 3h.

This complex-valued inverse Fourier transformation image reconstruction process can be equivalently described as a linear transformation with a real-valued representation [14]. Such a transformation is often called an isomorphism in mathematics. Define a real-valued vector,  $s$ , to be a  $2p_x p_y$  dimensional vector of complex-valued spatial frequencies from an image where the first  $p_x p_y$  elements are the rows of the real part of the spatial frequency matrix,  $S_R$ , shown in Fig. 3c, and the second  $p_x p_y$  elements are the rows of the imaginary part of the spatial frequency matrix,  $S_I$ , shown in Fig. 3d. The real-valued vector of spatial frequencies is thus formed as  $s = \text{vec}(S_R^T, S_I^T)$ , where  $(S_R^T, S_I^T)$  is a  $p_x \times 2p_y$  matrix formed by joining the transpose of the real and imaginary parts of  $S_C$  as seen in Fig. 4a, and  $\text{vec}(\cdot)$  denotes the vectorization operator that stacks the columns, shown in Fig. 4b, of its matrix argument. This yields us a real-valued vector representation of the matrix of spatial frequency ( $k$ -space) values that is given in Fig. 5b.

Further define a matrix  $\Omega$  that is another representation of the complex-valued inverse Fourier transformation matrices as described in Eq. (3) where the matrix elements of  $\Omega$  are

$$\begin{aligned}\Omega_R &= [(\Omega_{yR} \otimes \Omega_{xR})(\Omega_{yR} \otimes \Omega_{xR})] \\ \Omega_I &= [(\Omega_{yR} \otimes \Omega_{xR}) + (\Omega_{yI} \otimes \Omega_{xI})]\end{aligned}$$

and  $\otimes$  denotes the Kronecker product that multiplies every element of its first matrix argument by its entire second matrix argument. Utilizing the complex-valued Fourier matrix  $\Omega_{Cy}$ , with real and imaginary parts  $\Omega_{yR}$  and  $\Omega_{yI}$  given in Fig. 3a and Fig. 3b, along with the complex-valued Fourier matrix  $\Omega_{Cx}$ , with real and imaginary parts  $\Omega_{xR}$  and  $\Omega_{xI}$  given in Fig. 3e and Fig. 3f, the resulting  $\Omega$  matrix is presented in Fig. 5a.

The real-valued vector representation  $s$  of the spatial frequency ( $k$ -space) values in Fig. 5b is then pre-multiplied by the (inverse Fourier) reconstruction matrix  $\Omega$  as in Eq. (3)

$$\begin{aligned}r &= \Omega s \\ \begin{pmatrix} r_R \\ r_I \end{pmatrix} &= \begin{pmatrix} \Omega_R & \Omega_I \\ \Omega_I & \Omega_R \end{pmatrix} \begin{pmatrix} s_R \\ s_I \end{pmatrix}\end{aligned}\quad (3)$$

where the real-valued representation,  $r$ , of the complex-valued image has a dimension of  $2p_x p_y \times 1$ , true mean and no measurement error.

This is pictorially represented in Fig. 5. Fig. 5b is the spatial frequency vector  $s$  and Fig. 5a is the inverse Fourier transformation matrix  $\Omega$  as described in Eq. (3). This matrix multiplication produces a vector representation,  $r$ , of the image voxel measurements given in Fig. 5c as described in Eq. (3). The vector of voxel measurements,  $r$ , is partitioned into column blocks of length  $p_x$ . These blocks are then arranged as in Fig. 6a and formed into a single matrix image as in Fig. 6b where the first (last) eight columns are the transpose of the real (imaginary) part of the image. As can be seen, the same resultant complex-valued image is reconstructed with the complex-valued inverse Fourier transformation procedure described in Eq. (2) and presented in Fig. 3.

In the above described procedure, measurement noise was not considered. Redefine  $S_C$  to be the  $p_y \times p_x$  dimensional complex-valued spatial frequency measurement of a slice with noise

that consists of a  $p_y \times p_x$  dimensional matrix of true underlying noiseless complex-valued spatial frequencies,  $S_{0C}$ , and a  $p_y \times p_x$  dimensional matrix of complex-valued measurement error,  $E_C$ . This partitioning of the measured spatial frequencies in terms of true noiseless spatial frequencies plus measurement error can be represented as

$$S_C = (S_{0R} + iS_{0I}) + (E_R + iE_I) \quad (4)$$

where  $i$  is the imaginary unit while  $S_{0R}$ ,  $S_{0I}$ ,  $E_R$ , and  $E_I$  are real and imaginary matrix valued parts of the true spatial frequencies and measurement noise, respectively. Let  $\Omega_{Cx}$  and  $\Omega_{Cy}$  be  $p_x \times p_x$  and  $p_y \times p_y$  complex-valued Fourier matrices as described above. Then, the  $p_y \times p_x$  complex-valued inverse Fourier transformation reconstructed image,  $R_C$ , of  $S_C$  can be written as

$$\begin{aligned} R_C &= \Omega_{yC} S_C \Omega_{xC}^T \\ &= \Omega_{yC} (S_{0R} + iS_{0I}) \Omega_{xC}^T + \Omega_{yC} (E_R + iE_I) \Omega_{xC}^T \\ &= R_{0C} + iN_C \end{aligned} \quad (5)$$

where  $R_C$  has a true mean  $R_{0C}$  and measurement error  $N_C$ . Note that the complex-valued matrices for reconstruction,  $\Omega_x$  and  $\Omega_y$  in Eq. (5), need not be exactly Fourier matrices but may be Fourier matrices that include adjustments for independently measured magnetic field inhomogeneities or reconstruction matrices for other encoding procedures.

The real-valued inverse Fourier transformation method for image reconstruction can also be directly applied to noisy measurements. We can represent the noisy complex-valued spatial frequency matrix as  $s = s_0 + \varepsilon$  where this  $2p_x p_y$  dimensional vectors includes the reals of the rows stacked upon the imaginaries of the rows of the corresponding matrix. This implies that if the mean and covariance of the spatial frequency measurement vector,  $s$ , that is of dimension  $2p_x p_y \times 1$ , are  $s_0$  and  $\Gamma$ , then the mean and covariance of the reconstructed voxel measurements,  $r$ , are  $\Omega s_0$  and  $\Omega \Gamma \Omega^T$ .

### 3. Theory

The previously described data for a single image is expanded upon to mimic an fMRI experiment. In fMRI, a series of the previously described image slices are acquired. Denote the  $p_y \times p_x$  complex-valued spatial frequency matrix, corrupted by random noise, acquired at time  $t$  as  $S_{Ct} = S_{0Ct} + E_{Ct}$  and define  $S_t = \text{vec}(S_{Rt}^T, S_{It}^T)$ , where  $S_{Rt}$  and  $S_{It}$  are the real and imaginary parts of  $S_{Ct}$  for time points  $t=1, \dots, n$ . Define the total number of voxels in the image, which is the same as the number of complex-valued  $k$ -space measurements in fully sampled, Fourier encoded, Cartesian acquisitions, to be  $p = p_x p_y$ . This sequence of measured spatial frequency vectors can be collected into a  $2p \times n$  matrix  $S = (s_1, \dots, s_n)$  where the  $t^{\text{th}}$  column contains the  $p$  real  $k$ -space measurements stacked upon the  $p$  imaginary  $k$ -space measurements for time  $t$ . Having done this,  $n$  reconstructed images can be formed by the  $2p \times n$  matrix  $R = \Omega S$  where the  $t^{\text{th}}$  column of  $R$  contains the  $p$  real voxel measurements stacked upon the  $p$  imaginary voxel measurements for time  $t$ ,  $t=1, \dots, n$ .

The  $k$ -space measurements and the image voxel measurements can be stacked as  $s = \text{vec}(S)$  and  $r = \text{vec}(R)$ . Note that  $s$  and  $r$  have been redefined from their initial definition. If the mean and covariance of the  $2np \times 1$  vector of spatial frequency measurements,  $s$ , are  $s_0$  and  $\Delta$ , then the mean and covariance of the  $2np \times 1$  vector of reconstructed voxel measurements,  $r$ , are  $(I_n \otimes \Omega) s_0$  and  $(I_n \otimes \Omega) \Delta (I_n \otimes \Omega^T)$ . For example, if the  $k$ -space measurements were taken to be

temporally independent, then  $\Delta = I_n \otimes \Gamma$  and  $\text{cov}(r) = I_n \otimes (\Omega \Gamma \Omega^T)$ , where  $\Gamma$  is the covariance matrix for one  $k$ -space acquisition. Thus, we have described the fMRI voxel measurements as a linear function of the fMRI  $k$ -space measurements.

We can alternatively organize the voxel measurements by stacking the first set of  $p$  columns of  $R^T$  upon the second set of  $p$  columns of  $R^T$  to form a matrix  $Y$  of dimension  $2n \times p$ . Having done this, the  $j^{\text{th}}$  column of the resulting data matrix  $Y$  contains the  $n$  real voxel measurements stacked upon the  $n$  imaginary voxel measurements for voxel  $j$ ,  $j=1, \dots, p$ . The voxel measurements  $Y$  can be described with the complex fMRI model [12] as

$$Y = \left[ \begin{pmatrix} C_1 X \beta_1 \\ S_1 X \beta_1 \end{pmatrix}, \dots, \begin{pmatrix} C_p X \beta_p \\ S_p X \beta_p \end{pmatrix} \right] + \left[ \begin{pmatrix} \eta_{R1} \\ \eta_{I1} \end{pmatrix}, \dots, \begin{pmatrix} \eta_{Rp} \\ \eta_{Ip} \end{pmatrix} \right] \quad (6)$$

where  $C_1$  and  $S_1$  are diagonal matrices with cosine and sine terms respectively. Different activation models are found from Eq. (6) by different choices of the  $C$  and  $S$  matrices. The complex constant phase model [11] can be found with  $C_j = I_n \cos \theta_j$  and  $S_j = I_n \sin \theta_j$  where  $j$  indexes the  $j^{\text{th}}$  voxel. The unrestricted phase or magnitude only model can be found by selecting the  $t^{\text{th}}$  element of  $C_j$  and  $S_j$  to be  $C_{jt} = \cos \theta_{jt}$  and  $S_{jt} = \sin \theta_{jt}$ , where  $\theta_{jt}$  is unique for each  $j$  and  $t$ . The complex model for both magnitude and phase [9] can be found by choosing the phase  $\theta_{jt} = u_t^T \gamma_j$  where  $u_t$  is the  $t^{\text{th}}$  row of a phase design matrix  $U$  and  $\gamma_j$  are phase regression coefficients for voxel  $j$ .

Equation 6 can be rearranged and written with  $y = \text{vec}(Y)$  as

$$\begin{bmatrix} \begin{pmatrix} y_{R1} \\ y_{I1} \\ \vdots \\ y_{Rp} \\ y_{Ip} \end{pmatrix} \end{bmatrix} = \begin{bmatrix} \begin{pmatrix} C_1 X & 0 \\ 0 & S_1 X \end{pmatrix} & & 0 \\ & \ddots & \\ 0 & & \begin{pmatrix} C_p X & 0 \\ 0 & S_p X \end{pmatrix} \end{bmatrix} \begin{bmatrix} \begin{pmatrix} \beta_1 \\ \beta_1 \\ \vdots \\ \beta_p \\ \beta_p \end{pmatrix} \end{bmatrix} + \begin{bmatrix} \begin{pmatrix} \eta_{R1} \\ \eta_{I1} \\ \vdots \\ \eta_{Rp} \\ \eta_{Ip} \end{pmatrix} \end{bmatrix} \quad (7)$$

where  $y = (y_{R1}^T, y_{I1}^T, \dots, y_{Rp}^T, y_{Ip}^T)^T$  is a vector containing the real and imaginary reconstructed voxel measurements and  $\eta = (\eta_{R1}^T, \eta_{I1}^T, \dots, \eta_{Rp}^T, \eta_{Ip}^T)^T$  is a vector containing the real and imaginary errors of the reconstructed voxel measurements. The model can simply be written as  $y = \mu + \epsilon$ . For example, with constant phase model, the mean is

$$\mu = (I_2 \otimes X) [(\cos \theta_1, \sin \theta_1) \otimes \beta, \dots, (\cos \theta_p, \sin \theta_p) \otimes \beta].$$

The rearrangement of the voxel measurements from  $r$  to  $y$  is a linear transformation and can be achieved through multiplication with a permutation matrix  $P$  (described in Appendix A and presented in Fig. 10) as  $y = Pr$ . In terms of the original  $k$ -space measurements the voxel time courses are  $y = P(I_n \otimes \Omega) \text{vec}[\text{vec}(S_{R1}^T, S_{I1}^T), \dots, \text{vec}(S_{Rn}^T, S_{In}^T)]$ . Having done this linear transformation, the mean and covariance of  $y$  are  $\mu = P(I_n \otimes \Omega) s_0$  and  $\Lambda = P(I_n \otimes \Omega) \Delta (I_n \otimes \Omega^T) P^T$ . Since the matrices  $\Omega$  and  $P$  that convert  $k$ -space measurements,  $s$ , to voxel measurements,  $y$ , are known *a priori*, the expression  $y = P(I_n \otimes \Omega) s$  can be inverted to write  $s = (I_n \otimes \Omega^{-1}) P^{-1} y$ , and in terms of the parameters as



$$\begin{pmatrix} s_1 \\ \vdots \\ s_n \end{pmatrix} = \underbrace{(\mathbf{I}_n \otimes \boldsymbol{\Omega}^1) \mathbf{P}^1 (\mathbf{I}_{2n} \otimes \mathbf{X})}_{\text{known}} \begin{pmatrix} \beta_1 \cos \theta_1 \\ \beta_1 \sin \theta_1 \\ \vdots \\ \beta_p \cos \theta_p \\ \beta_p \sin \theta_p \end{pmatrix} + \begin{pmatrix} \varepsilon_1 \\ \vdots \\ \varepsilon_n \end{pmatrix} \quad (8)$$

Thus the optimization for the regression coefficients ( $\beta$ ) and phases ( $\theta$ ) in Eq. (8) can be performed in  $k$ -space to yield the same parameter estimates as the standard method. Activations can then be computed from the described complex activation models.

Using ordinary least squares or a normal distributional specification on the errors, the voxel-wise regression coefficients and phases can be determined to yield the same point estimators as in Rowe and Logan [11]. The Rowe-Logan unconstrained alternative hypothesis estimators (with hats) for  $H_1: C\beta \neq 0$  along with the constrained null hypothesis estimators (with tildes) for  $H_0: C\beta = 0$  in voxel  $j$  are

$$\begin{aligned} \hat{\theta}_j &= \frac{1}{2} \tan^{-1} \left[ \frac{\hat{\beta}_{Rj}^T (X^T X) \hat{\beta}_{Ij}}{(\hat{\beta}_{Rj}^T (X^T X) \hat{\beta}_{Rj} + \hat{\beta}_{Ij}^T (X^T X) \hat{\beta}_{Ij})/2} \right] & \tilde{\theta}_j &= \frac{1}{2} \tan^{-1} \left[ \frac{\tilde{\beta}_{Rj}^T (X^T X) \tilde{\beta}_{Ij}}{(\tilde{\beta}_{Rj}^T (X^T X) \tilde{\beta}_{Rj} + \tilde{\beta}_{Ij}^T (X^T X) \tilde{\beta}_{Ij})/2} \right] \\ \hat{\beta}_j &= \hat{\beta}_{Rj} \cos(\hat{\theta}_j) + \hat{\beta}_{Ij} \sin(\hat{\theta}_j) & \tilde{\beta}_j &= \tilde{\beta}_{Rj} \cos(\tilde{\theta}_j) + \tilde{\beta}_{Ij} \sin(\tilde{\theta}_j) \end{aligned} \quad (9)$$

where  $C$  is an  $r \times (q+1)$  matrix of full row rank,  $\psi = \mathbf{I}_{q+1} - (X^T X)^{-1} C^T [C(X^T X)^{-1} C^T]^{-1} C$ ,  $\hat{\beta}_{Rj} = (X^T X)^{-1} X^T y_{Rj}$ , and  $\hat{\beta}_{Ij} = (X^T X)^{-1} X^T y_{Ij}$ , while  $y_{Rj}$  and  $y_{Ij}$  are the  $n \times 1$  vectors of real and imaginary voxel observations.

We can convert from the vector  $r$ , which is presented in Fig. 10c, to the vector  $y$ , which is shown in Fig. 10a, via a permutation matrix  $P$ , a portion of which is displayed in Fig. 10b. Now with the  $y$  vector being arranged as real and imaginary observations in each voxel as described in Eq. (7), we can apply the complex activation models [11]. The regression coefficients  $\beta$ , the phase angle  $\theta$ , and the variance  $\sigma^2$  are estimated under both the null and alternative hypotheses as described in Eq. (9) then activation computed.

Voxel-wise activations are the same as in Rowe and Logan [11]. Then the generalized

likelihood ratio statistic for the complex fMRI activation model is  $2 \log \lambda_j = 2n(\tilde{\sigma}_j^2 / \hat{\sigma}_j^2)$ . This statistic has a large sample  $\chi_r^2$  distribution. Note that when  $r=1$ , two-sided testing can be done using the signed likelihood ratio test given by

$$Z_j = \text{sign}(C\hat{\beta}_j) \sqrt{2 \log \lambda_j}, \quad (10)$$

which has a large sample standard normal distribution under the null hypothesis. Alternatively with  $r=1$ , a Wald type statistic can be formed

$$w_j = C\hat{\beta}_j / \sqrt{\hat{\sigma}_j^2 C(X^T X)^{-1} C^T}, \quad (11)$$

which also has a large sample standard normal distribution under the null hypothesis. A map of these activation statistics from either Eq. 10 or Eq. 11 is then thresholded while adjusting for multiple comparisons [6,7]. However, correlations between voxels are characterized in terms of spatio-temporal correlations between  $k$ -space measurements.

The variances and covariances in the spatio-temporal domain in an example with a specification of uncorrelated temporal  $k$ -space measurement vectors ( $s_t$ ) are included in the covariance matrix  $\Lambda = P(I_n \otimes \Omega \Gamma \Omega^T) P^T$  for the voxel measurements. Define the voxel measurement covariance matrix to be  $\Sigma$ . Having estimated the voxel-wise regression coefficients and phases, we can estimate the mean of the vector of voxel measurements  $y$  by  $\hat{\mu}$  (under the alternative hypothesis) and the mean of the matrix of voxel measurements  $R$  by  $\hat{M} = \text{vec}^{-1}(P^{-1} \hat{\mu})$ . Here  $\text{vec}^{-1}(\cdot)$  is the operator that is the inverse operation of the  $\text{vec}(\cdot)$  operator. The voxel covariance matrix  $\Sigma$  can now be estimated by  $\hat{\Sigma} = (R - \hat{M})(R - \hat{M})^T/n$ .

With the physically motivated specification of the same voxel covariance,  $\Sigma_W$ , within the real-imaginary channels and voxel covariance,  $\Sigma_B$ , between the real-imaginary channels, the previous the voxel covariance matrix becomes

$$\Sigma = \begin{bmatrix} \Sigma_W & \Sigma_B \\ \Sigma_B & \Sigma_W \end{bmatrix} \quad (12)$$

We can estimate the covariance matrices in Eq. (12) under the alternative hypothesis by

$$\begin{aligned} \hat{\Sigma}_W &= [(R_R \hat{M}_R)(R_R \hat{M}_R)^T + (R_I \hat{M}_I)(R_I \hat{M}_I)^T]/(2n) \\ \hat{\Sigma}_B &= [(R_R \hat{M}_R)(R_I \hat{M}_I)^T + (R_I \hat{M}_I)(R_R \hat{M}_R)^T]/(2n) \end{aligned} \quad (13)$$

and under the null hypothesis similarly find  $\tilde{\Sigma}_W$  and  $\tilde{\Sigma}_B$  by replacing hats in Eq. (13) with tildes. It should be noted that the  $j^{\text{th}}$  diagonal elements of  $\tilde{\Sigma}_W$  are equivalent to those given in Rowe and Logan [11] where the estimate under the alternative hypothesis is

$$\tilde{\sigma}_j^2 = \frac{1}{2} \begin{bmatrix} y_{Rj} X \hat{\beta}_j \cos \hat{\theta}_j \\ y_{Ij} X \hat{\beta}_j \sin \hat{\theta}_j \end{bmatrix}^T \begin{bmatrix} y_{Rj} X \hat{\beta}_j \cos \hat{\theta}_j \\ y_{Ij} X \hat{\beta}_j \sin \hat{\theta}_j \end{bmatrix} \quad (14)$$

and under the null hypothesis is similarly,  $\tilde{\sigma}_j^2$  found by replacing hats in Eq. (14) with tildes. As described in Eq. (13), we can also estimate covariance between voxels,  $\hat{\Sigma}$ .

## 4. Methods

As before, this time series procedure can be represented pictorially. The complex-valued image in Fig. 2c and Fig. 2d was taken as the mean “active” or “on” image and a duplicate of it with the two white voxels replaced by grey voxels were used as the mean “inactive” or “off” images. For illustrative purposes, an experiment with eight blocks where each block consists of eight on images followed by eight off images is initially presented. Subsequently all eight blocks were examined. Eight column vectors of the spatial frequencies for the true mean “on” image were joined into a matrix with eight column vectors of the spatial frequencies for the true mean “off” image as in Fig. 7b. Each column in Fig. 7b is the vector form of the spatial frequencies for an image similar to that in Fig. 5b.



The mean “on” images contained voxels with values  $\beta_0=0$  and  $\beta_1=0$  outside a four by four by four internal region, inactive gray voxels within the four by four region with values  $\beta_0=\text{SNR}\cdot\sigma$  and  $\beta_1=0$ , along with two active voxels with value  $\beta_0=\text{SNR}\cdot\sigma$  and  $\beta_1=\text{CNR}\cdot\sigma$ . Activation parameter values were  $\text{SNR}=30$ ,  $\text{CNR}=1$  and  $\sigma=.05$ . In this parameterization, SNR denotes the temporal signal-to-noise ratio, CNR denotes the functional contrast-to-noise ratio, and  $\sigma$  denotes the voxel standard deviation.

Independent noise column vectors  $\epsilon_t$ , as seen in Fig. 7c, were generated from a normal distribution with zero mean vector and covariance matrix  $\Gamma=\gamma^2\Gamma_1 \otimes \Gamma_2 \otimes \Gamma_3$ . This covariance structure mimics temporal autocorrelation along the echo planar imaging (EPI) trajectory along with correlation between real and imaginary parts. The covariance matrix was formed with  $\Gamma_1$ ,  $\Gamma_2$ , and  $\Gamma_3$  taken to be unit variance correlation matrices while  $\gamma$  was taken to be  $\gamma^2=p_x p_y \sigma^2$ . The  $p_y \times p_y$  correlation matrix  $\Gamma_1$  is taken to be an AR(1) correlation matrix with  $(i,j)^{\text{th}}$  element  $\psi_1^{|i-j|}$  where  $\psi_1=0.25$ , the  $2 \times 2$  correlation matrix  $\Gamma_2$  is taken to have an off diagonal correlation of  $\psi_2=0.5$  while the  $p_x \times p_x$  correlation matrix  $\Gamma_3$  is taken to be an AR(1) correlation matrix with  $(i,j)^{\text{th}}$  element  $\psi_3^{|i-j|}$  where  $\psi_3=0.5$ .

## 5. Results

Each matrix image in Fig. 7a, b, and c was pre-multiplied by the (inverse Fourier transform) image reconstruction matrix  $\Omega$ , given in Eq. (3) and presented in Fig. 5a. The results of this pre-multiplication can be seen in Fig. 8a, b, and c. The columns of  $R=\Omega S$  in Fig. 8a are real and imaginary parts for each noisy image. The noisy image in Fig. 8a is the sum of the noiseless image in Fig. 8b and the measurement noise image in Fig. 8c. However, the real and imaginary parts for each noisy voxel are useful for considering activation. As described in Section 3, one can vectorize  $R$  and  $S$  to yield  $r=\text{vec}(R)$  and  $s=\text{vec}(S)$  as seen in Fig. 9. The vector  $s$  of noisy spatial frequency ( $k$ -space) values, as presented in Fig. 9c, is pre-multiplied by a block diagonal matrix with  $\Omega$  along the diagonal, as displayed in Fig. 9b, to produce a vector of noisy image measurements,  $r$ , as shown in Fig. 9a.

In Fig. 11a and Fig. 11c are the unthresholded activation maps for the magnitude-only and complex-valued activation methods respectively. In Fig. 11b and d are the Bonferroni 5% thresholded activation maps for the magnitude-only and complex-valued activation techniques respectively. Note the spurious activation from the magnitude-only method as a result of its suboptimal parameterization [9].

The sample voxel correlation from  $\hat{\Sigma}_W$  described in Eq. (13) is displayed in Fig. 12a with theoretical values presented in Fig. 12b. The sample correlation from  $\hat{\Gamma}=\Omega^{-1} \hat{\Sigma}(\Omega^T)^{-1}$  is given in Fig. 12c with theoretical values in Fig. 12d. Note the similarity between the sample values and the theoretical values in Fig. 11a and Fig. 11c to the theoretical values in Fig. 11b and Fig. 11d even for the small sample size.

## 6. Discussion

A linear representation of image reconstruction has been presented, and that reconstruction operation has been included into the complex-valued general linear model for fMRI. This parameterization of the complex-valued general linear model allows one to compute activations directly from  $k$ -space measurements. This offers some advantages. The previously separate, tedious processes of image reconstruction and functional analysis can now be considered in one step. As the reconstruction matrix, permutation matrix, and design matrix (marked “known” in Equation 8) are all known, their product may be computed once for a given

experiment. Thus, the determination of image-space regression coefficients can be made with one matrix multiplication on the acquired  $k$ -space data vector.

Of course, some data processing is more naturally performed in image-space. An example of such processing is motion correction. In that case, a matrix which shifts and/or rotates the reconstructed image can be used to multiply the reconstruction operator. Thus, the processed and reconstructed data would be the result of two matrices multiplying the acquired  $k$ -space data in this linear representation.

Furthermore, in light of this parameterization, the spatio-temporal covariances between the complex-valued voxel measurements,  $\Lambda$ , can now be described in terms of the spatio-temporal covariances between the complex-valued  $k$ -space measurements,  $\Delta$ . The covariance of the complex-valued  $k$ -space measurements may be due to independent sources, such as spatio-temporal independent noise  $\Delta_I$  and true physiologic processes  $\Delta_P$ , so that  $\Delta = \Delta_P + \Delta_I$ . Adjustments to the  $k$ -space measurements could modify the correlation structure. These  $k$ -space adjustments can be written as  $s_A = A s = A(s_0 + \varepsilon) = A s_0 + A \varepsilon$  and  $r_A = \Omega A(s_0 + \varepsilon) = \Omega A s_0 + \Omega A \varepsilon$  where the subscript  $A$  denotes an adjusted measurement. Then the mean and variance/covariance matrices are  $E(s_A) = A s_0$  and  $\text{var}(s_A) = A \Gamma A^T$  for the spatial frequency measurements and  $E(r_A) = \Omega A s_0$  and  $\text{var}(r_A) = \Omega A \Gamma A^T \Omega^T$  for the voxel measurements. So unless  $\Gamma = I$  and  $A A^T = I$  the voxels are correlated because  $\Omega \Omega^T = I$ . Through reconstruction and other processing, one is changing the physiologic and independent correlations. They change according to

$$\begin{aligned} \text{var}(s) &= \Gamma_p + \Gamma_i & \rightarrow & \text{var}(s_A) = A \Gamma_p A^T + A \Gamma_i A^T \\ \text{var}(r) &= \Omega \Gamma_p \Omega^T + \Omega \Gamma_i \Omega^T & \rightarrow & \text{var}(r_A) = \Omega A \Gamma_p A^T \Omega^T + \Omega A \Gamma_i A^T \Omega^T \end{aligned}$$

It is possible that incomplete consideration of correlations induces undesirable correlations or obscures relevant correlations. Proper modeling suggests that one should adjust the covariance matrices in light of all data processing.

One could apply temporal filtering or pre-whitening to the  $k$ -space measurements that are residuals after fitting a regression model in image space. After fitting the fMRI model to the voxel image time courses, one can transform the residual images into spatial frequencies ( $k$ -space) and estimate the correlation due to adjustment sources  $A A^T$ . The spatial frequencies can then be temporally pre-whitened, transformed back into residual images then the noise variation  $\Sigma_W$  re-estimated.

As mentioned earlier, although only Cartesian Fourier reconstruction is described in this manuscript, any linear reconstruction method may be used in place of  $\Omega$ . This includes non-Cartesian sampling schemes, like spiral. Some new reconstruction operator,  $\omega$ , may be considered that is the product of two matrices which grid the data to the Cartesian grid and Fourier transform the Cartesian data. Sparsely sampled, multi-coil data may be considered with yet another reconstruction operator,  $\omega'$ , which generates the omitted data as a linear combination of the acquired multi-coil data and Fourier transforms the generated, fully sampled data.

In this work, complex-valued voxel measurements have been written in terms of the original complex-valued  $k$ -space measurements. This allows the computation of statistically significant fMRI brain activation in image space directly from the original  $k$ -space measurements. The correlation between voxel measurements can also be written in terms of correlation between  $k$ -space measurements. Since the covariance matrix between the  $k$ -space measurements, and hence voxel measurements, can be partitioned into individual sources of covariation, statistical

associations between individual voxels or regions of interest could be quantified utilizing unmodeled sources of covariation.

## Appendix A

The permutation matrix for rearranging values to be grouped by image to be grouped by voxel is described. A permutation matrix is a square matrix that can be obtained by permuting (rearranging) either the columns or rows of an identity matrix [3]. A permutation matrix is of full rank and therefore nonsingular and also invertible. Also note that a permutation matrix,  $P$ , is an orthogonal matrix so  $P^{-1}=P^T$  and  $PP^T=I$ . The elements of the permutation matrix  $P$  are all zero except for a single 1 in each row. The first  $n$  rows of the permutation matrix,  $P$ , forms the  $n$  real measurements of the first voxel. The  $t^{\text{th}}$  row,  $t=1, \dots, n$  within the first set of  $n$  rows of the permutation matrix,  $P$ , have a 1 in column  $t=0p+1, 2p+1, 4p+1, \dots, 2(n-1)p+1$ . The second  $n$  rows of the permutation matrix,  $P$ , forms the imaginary measurements in the first voxel. The  $t^{\text{th}}$  row within the second set of  $n$  rows of the permutation matrix  $P$  have a 1 in column  $t=p+1, 3p+1, 5p+1, \dots, 2(n-1)p+p+1$ . For the second voxel, the  $t^{\text{th}}$  row within the third set of  $n$  rows of the permutation matrix  $P$  have a 1 in column  $t=0p+2, 2p+2, 4p+2, \dots, 2(n-1)p+2$ . The  $t^{\text{th}}$  row within the fourth set of  $n$  rows of the permutation matrix  $P$  that form the  $n$  imaginary measurements within the second voxel have a 1 in column  $t=p+2, 3p+2, 5p+2, \dots, 2(n-1)p+p+2$ . This general pattern continues. In general, the  $j^{\text{th}}$  set of  $2n$  rows for the  $j^{\text{th}}$  voxel,  $j=1, \dots, p$  have a 1 in columns  $0p+j, 2p+j, 4p+j, \dots, 2(n-1)p+j$  of its first  $n$  rows for the real voxel measurements and in columns  $p+j, 3p+j, 5p+j, \dots, 2(n-1)p+p+j$  for the imaginary voxel measurements.

## Acknowledgments

This work was supported in part by NIH EB000215.

## References

1. Bandettini PM, Jesmanowicz A, Wong EC, Hyde JS. Processing strategies for time-course data sets in functional MRI of the human brain. *Magn Reson Med* 1993;30:161–173. [PubMed: 8366797]
2. Haacke, M.; Brown, R.; Thompson, M.; Venkatesan, R. *Magnetic resonance imaging: Physical principles and sequence design*. New York: John Wiley and Sons; 1999.
3. Harville, DA. *Matrix algebra from a statistician's perspective*. Springer-Verlag; New York: 1999.
4. Kumar A, Welti D, Ernst RR. NMR Fourier Zeugmatography. *J Magn Reson* 1975;18:69–83.
5. Lai S, Glover GH. Detection of BOLD fMRI signals using complex data. *Proc ISMRM* 1997;5:1671.
6. Logan BR, Rowe DB. An evaluation of thresholding techniques in fMRI analysis. *Neuroimage* 2004;22(1):95–108. [PubMed: 15110000]
7. Logan BR, Geliazkova MP, Rowe DB. An evaluation of spatial thresholding techniques in fMRI analysis. *Hum Brain Mapp* 2008;29(12):95–108.
8. Nan FY, Nowak RD. Generalized likelihood ratio detection for fMRI using complex data. *IEEE Trans Med Imag* 1999;8:320–329.
9. Rowe DB, Logan BR. A complex way to compute fMRI activation. *Neuroimage* 2004;23:1078–92. [PubMed: 15528108]
10. Rowe DB, Logan BR. Complex fMRI analysis with unrestricted phase is equivalent to a magnitude-only model. *Neuroimage* 2005;24(2):603–606. [PubMed: 15627605]
11. Rowe DB. Parameter estimation in the magnitude-only and complex-valued fMRI data models. *Neuroimage* 2005;25:1124–1132. [PubMed: 15850730]
12. Rowe DB. Modeling both the magnitude and phase of complex-valued fMRI data. *Neuroimage* 2005;25(4):1310–1324. [PubMed: 15850748]
13. Rowe DB, Meller CP, Hoffmann RG. Characterizing phase-only fMRI data with an angular regression model. *J Neurosci Methods* 2007;161(2):331–341. [PubMed: 17157916]

14. Rowe DB, Nencka AS, Hoffmann RG. Signal and noise of Fourier reconstructed fMRI data. *J Neurosci Methods* 2007;159(2):361–369. [PubMed: 16945421]

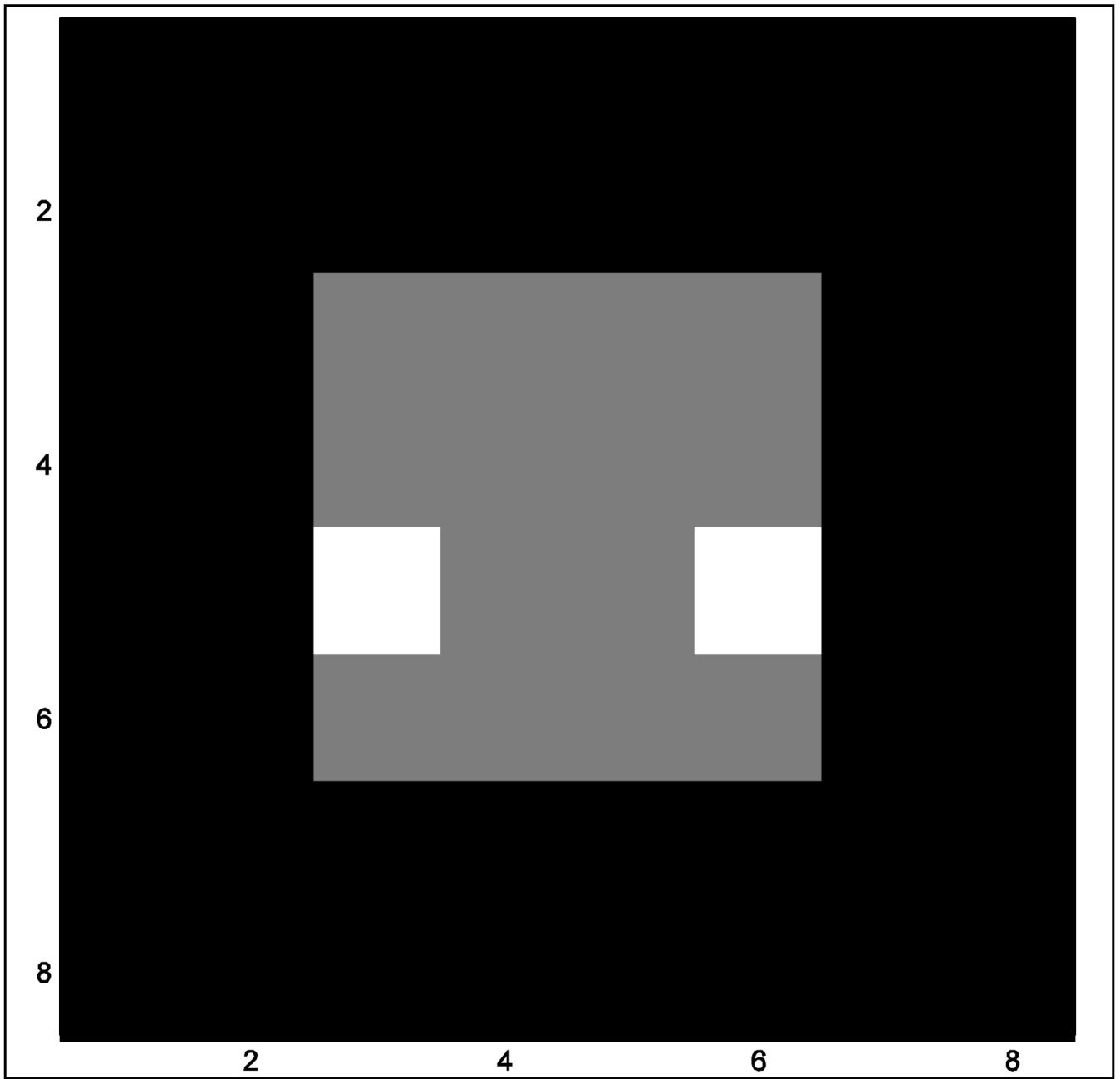


**Fig. 1.**  
Ideal noiseless image.

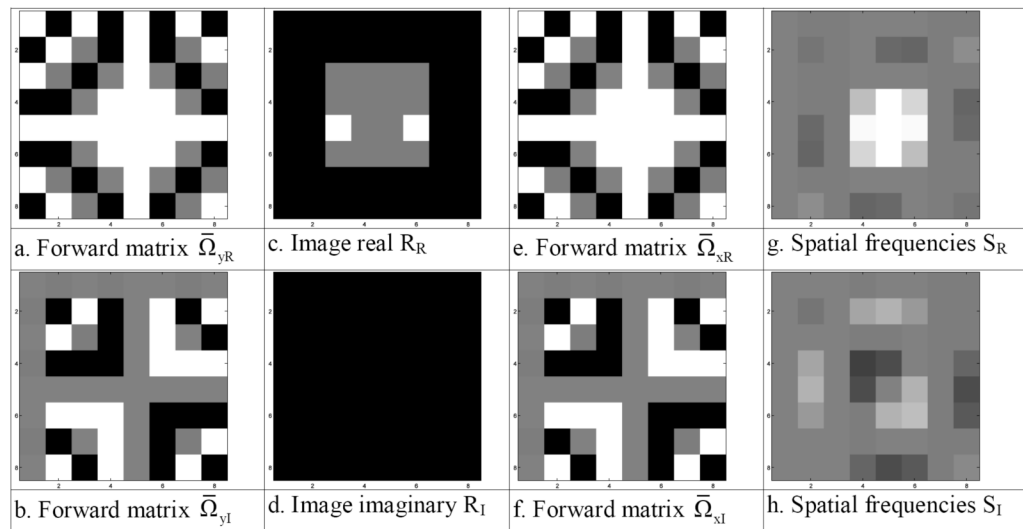


**Fig. 2.**  
Complex-valued 2D forward Fourier transform.

- a. Forward matrix  $\bar{\Omega}_{yR}$
- b. Forward matrix  $\bar{\Omega}_{yI}$
- c. Image real  $R_R$
- d. Image imaginary  $R_I$
- e. Forward matrix  $\bar{\Omega}_{xR}$
- f. Forward matrix  $\bar{\Omega}_{xI}$
- g. Spatial frequencies  $S_R$
- h. Spatial frequencies  $S_I$



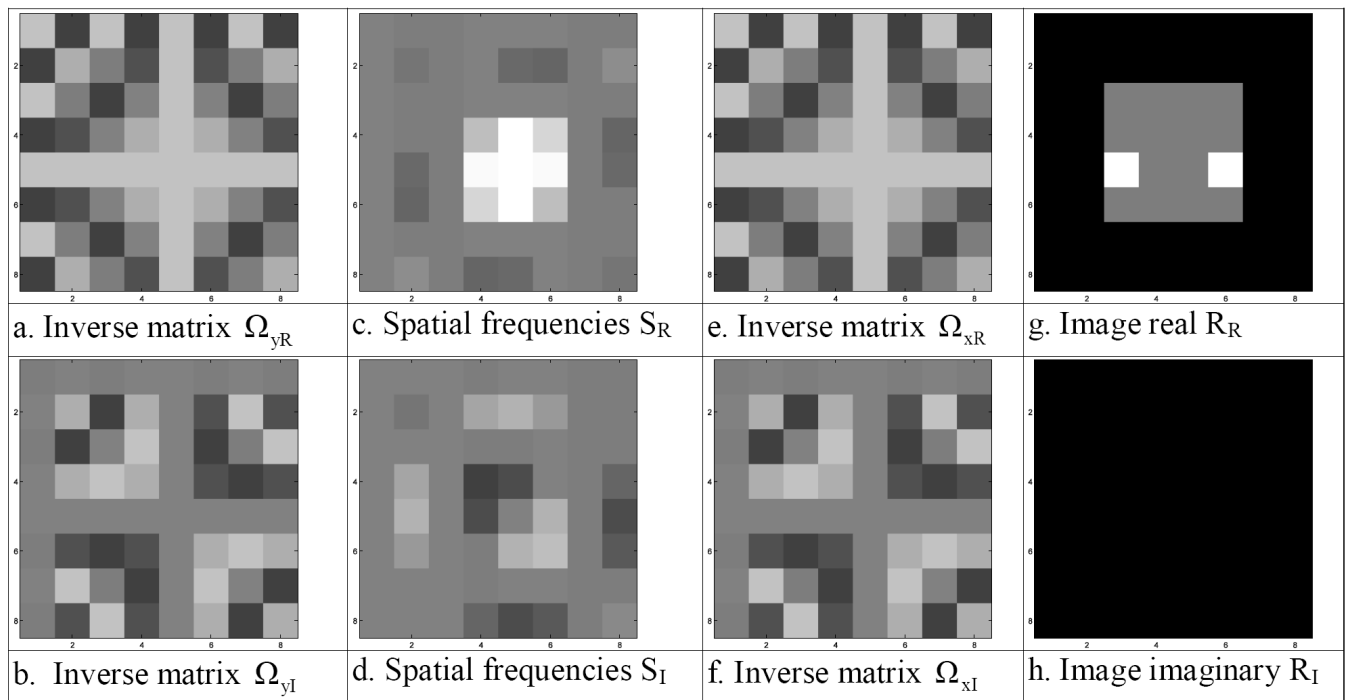


**Fig. 3.**  
Complex-valued 2D inverse Fourier transform.

- a. Inverse matrix  $\Omega_{yR}$
- b. Inverse matrix  $\Omega_{yI}$
- c. Spatial frequencies  $S_R$
- d. Spatial frequencies  $S_I$
- e. Inverse matrix  $\Omega_{xR}$
- f. Inverse matrix  $\Omega_{xI}$
- g. Image real  $R_R$
- h. Image imaginary  $R_I$

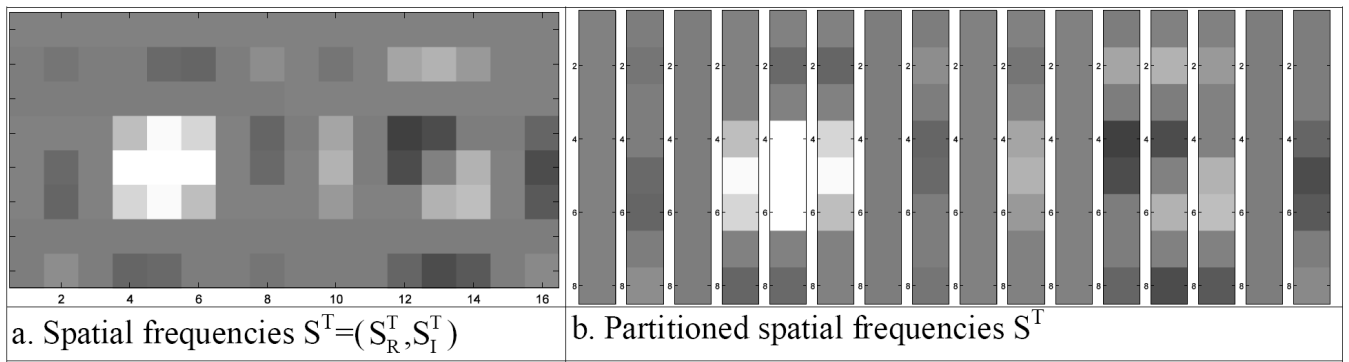


**Fig. 4.**  
Matrix to vector spatial frequency ( $k$ -space) values.

- a. Spatial frequencies  $S^T = (S_R^T, S_I^T)$
- b. Partitioned spatial frequencies  $S^T$

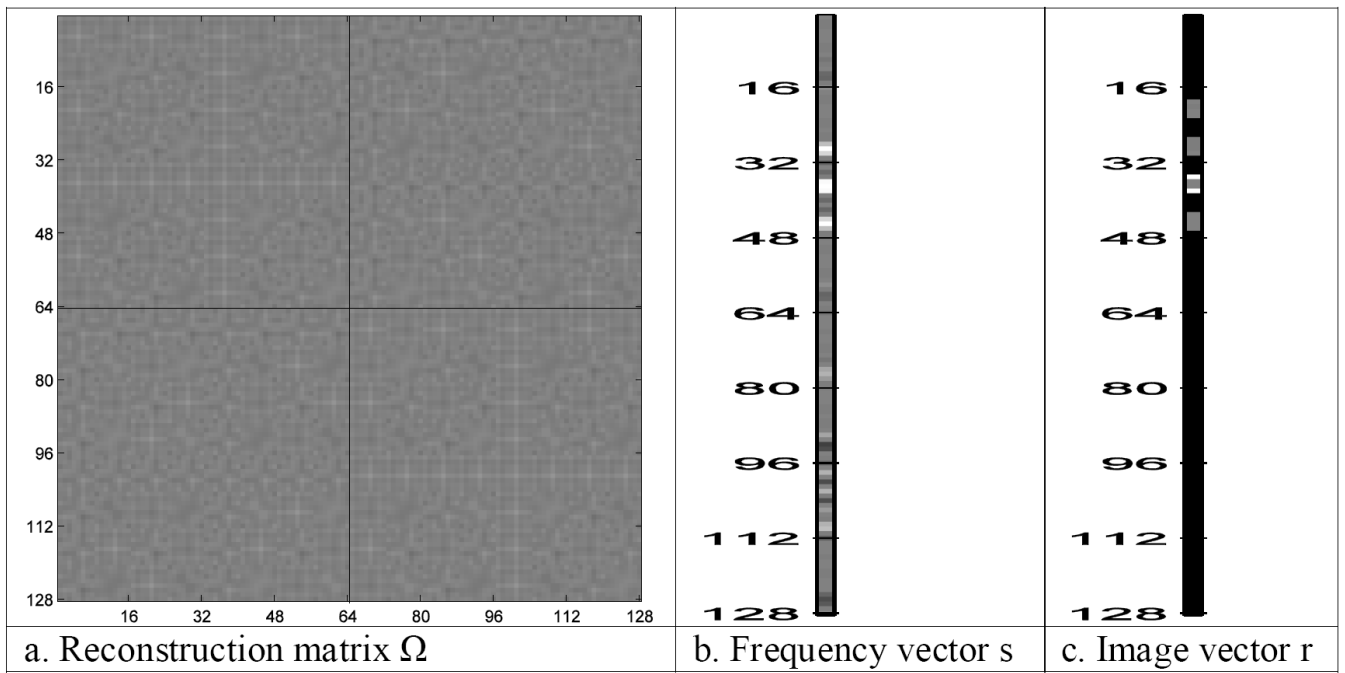


**Fig. 5.**  
Isomorphism for complex-valued 2D inverse Fourier Transform.

- a.** Reconstruction matrix  $\Omega$
- b.** Frequency vector  $s$
- c.** Image vector  $r$

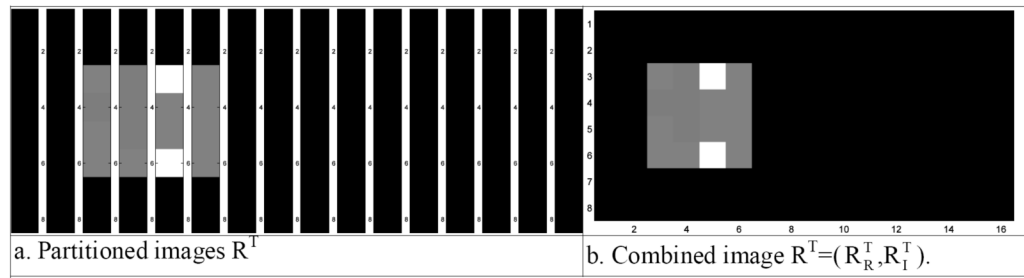


**Fig. 6.**  
Vector to matrix image values.

- a. Partitioned images  $R^T$
- b. Combined image  $R^T = (R_R^T, R_I^T)$

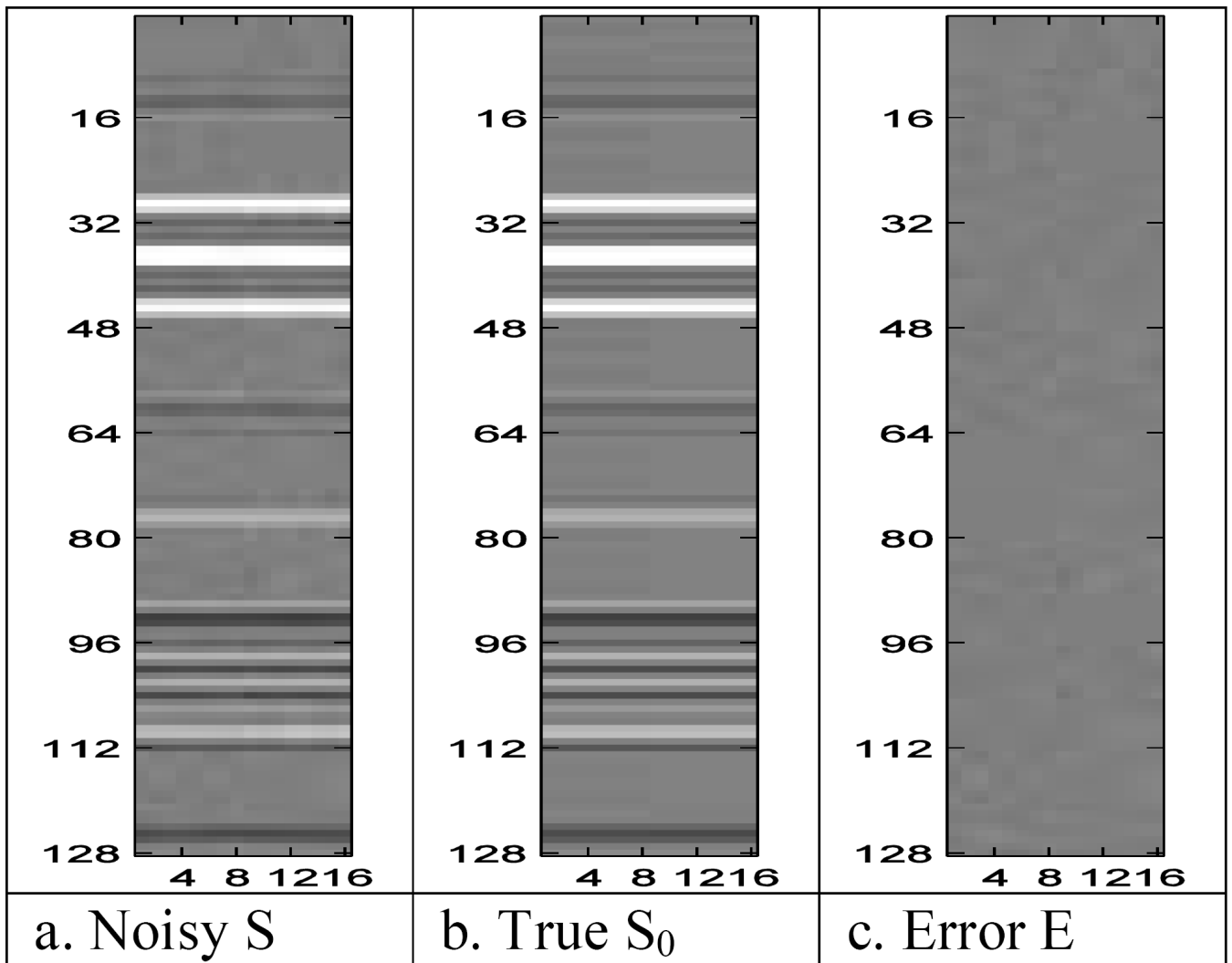


**Fig. 7.**  
Noisy spatial frequency ( $k$ -space) values.

- a. Noisy  $S$
- b. True  $S_0$
- c. Error  $E$

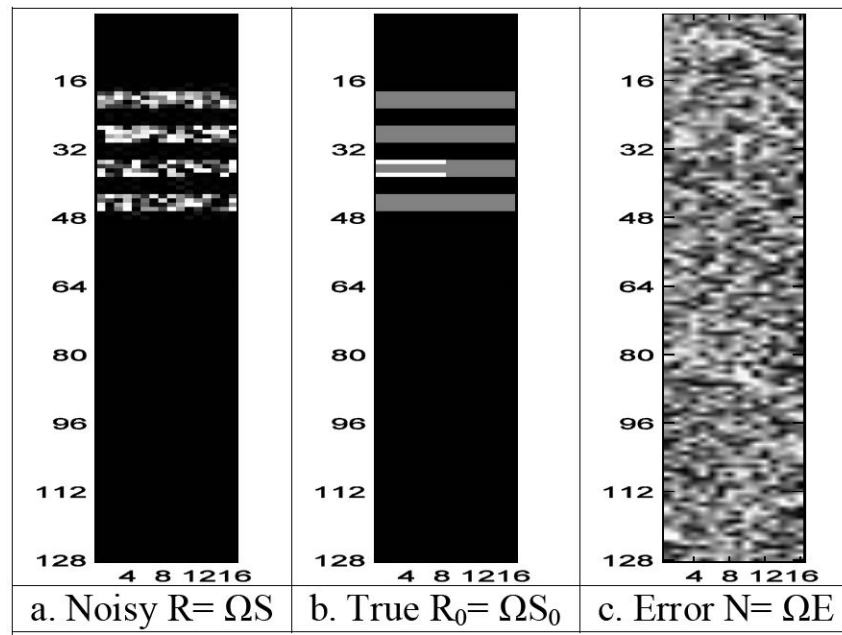


**Fig. 8.**  
Reconstructed noisy images.

- a. Noisy  $R = \Omega S$
- b. True  $R_0 = \Omega S_0$
- c. Error  $N = \Omega E$



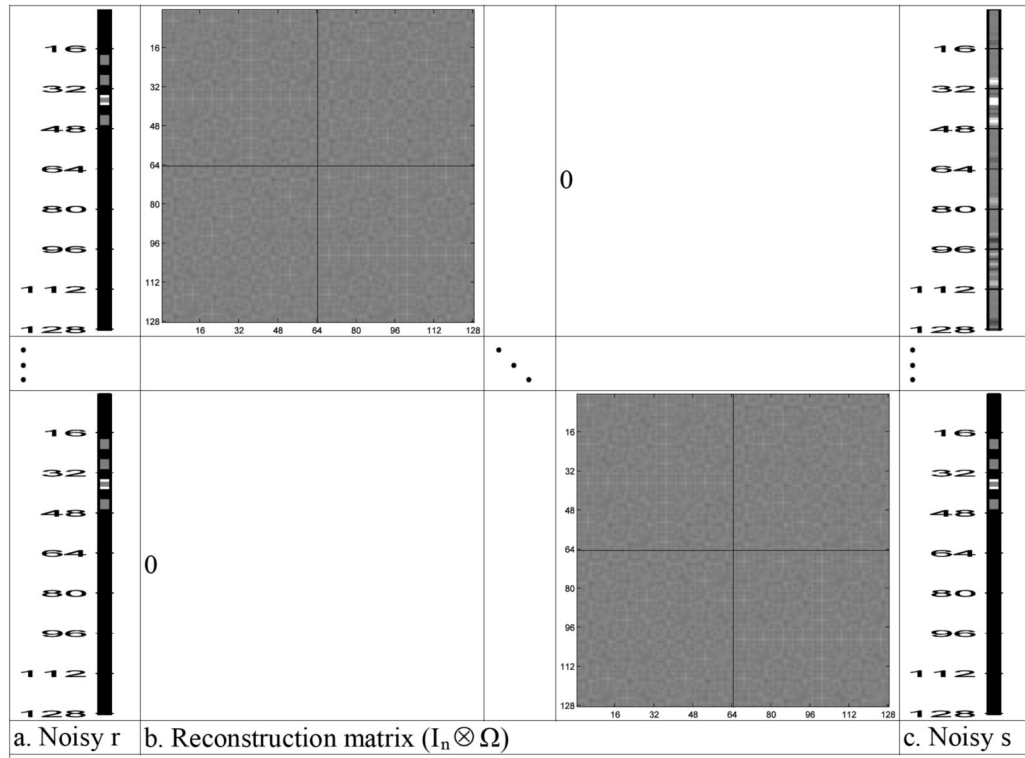


**Fig. 9.**  
Reconstructed vectorized noisy images.

- a. Noisy r
- b. Reconstruction matrix ( $I_n \otimes \Omega$ )
- c. Noisy s

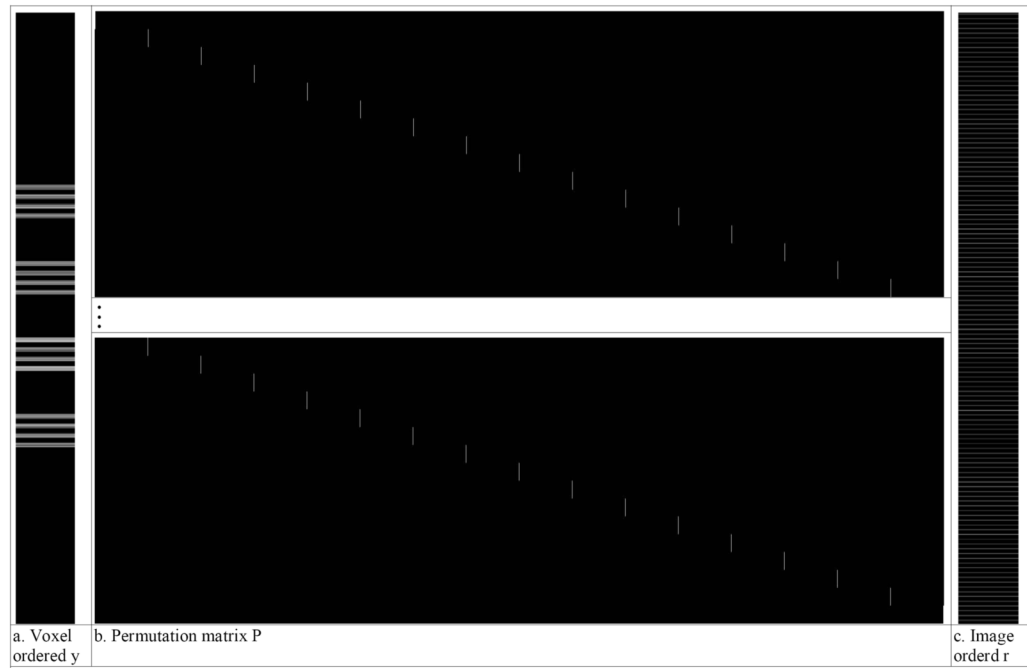


**Fig. 10.**  
Reordered reconstructed voxels.

- a. Voxel ordered y
- b. Permutation matrix P
- c. Image orderd r

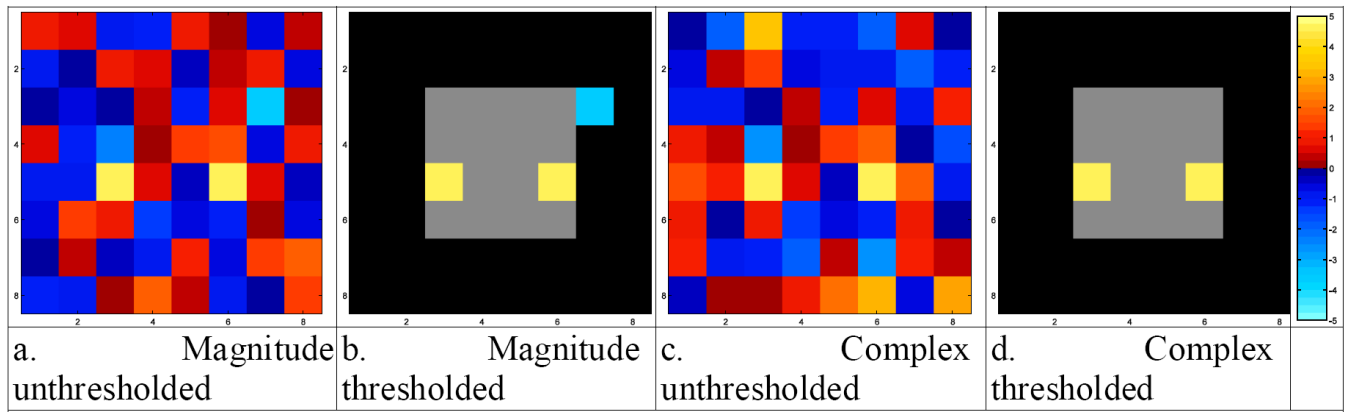


**Fig. 11.**  
Activation maps. Bonferroni 5% threshold.

- a. Magnitude unthresholded
- b. Magnitude thresholded
- c. Complex unthresholded
- d. Complex thresholded

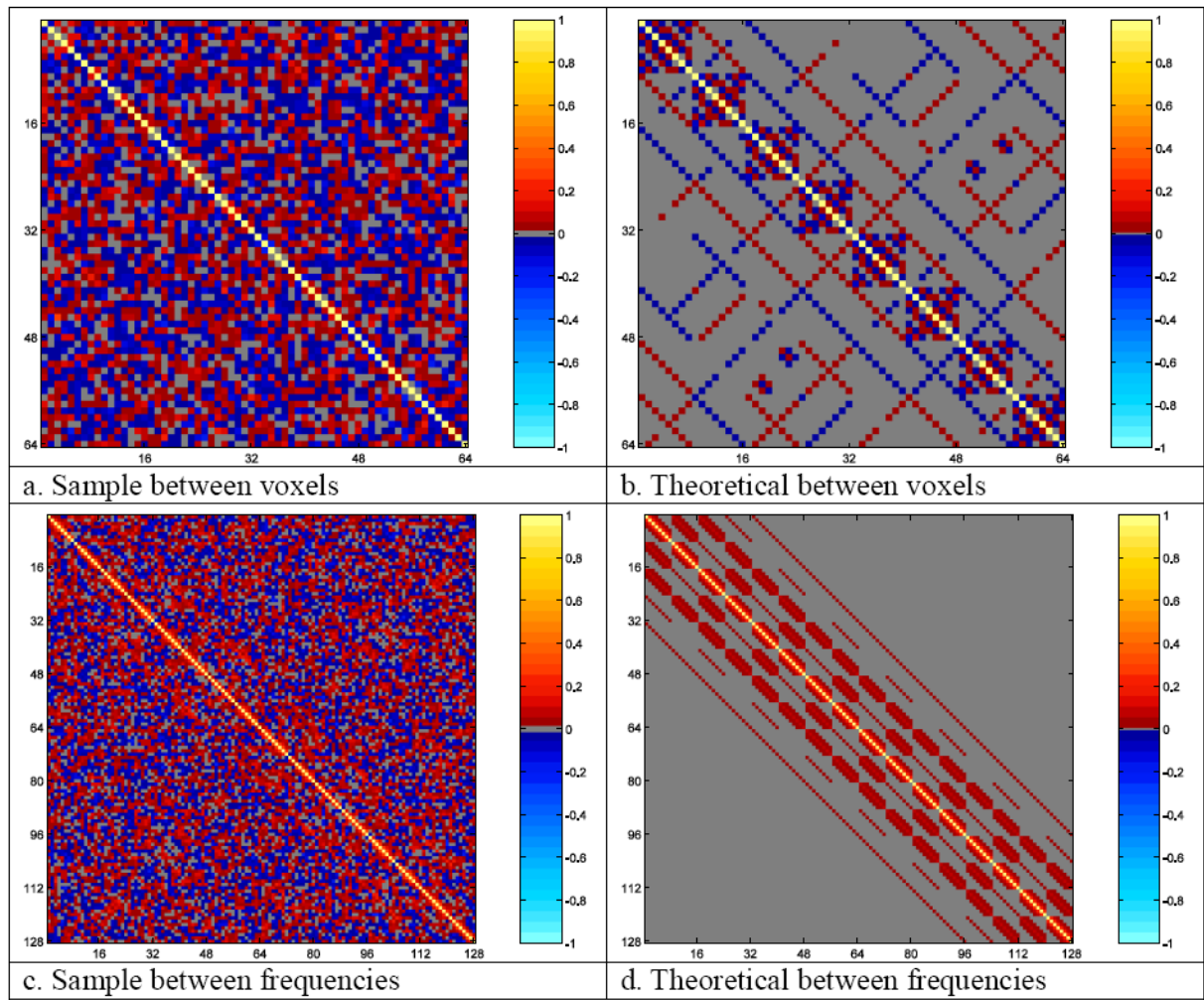


**Fig. 12.**  
Correlation matrices.

- a. Sample between voxels
- b. Theoretical between voxels
- c. Sample between frequencies
- d. Theoretical between frequencies